nature medicine

Inhibition of fatty acid oxidation as a therapy for MYC-overexpressing triple-negative breast cancer

Roman Camarda[1,2], Alicia Y Zhou[1], Rebecca A Kohnz[3], Sanjeev Balakrishnan[1], Celine Mahieu[1], Brittany Anderton[1,2], Henok Eyob[1], Shingo Kajimura[1,4,5], Aaron Tward[6], Gregor Krings[7], Daniel K Nomura[3] & Andrei Goga[1,8,9]

© 2016 Nature America, Inc. All rights reserved.

Expression of the oncogenic transcription factor MYC is disproportionately elevated in triple-negative breast cancer (TNBC), as compared to estrogen receptor–, progesterone receptor– or human epidermal growth factor 2 receptor–positive (RP) breast cancer[1,2]. We and others have shown that MYC alters metabolism during tumorigenesis[3,4]. However, the role of MYC in TNBC metabolism remains mostly unexplored. We hypothesized that MYC-dependent metabolic dysregulation is essential for the growth of MYC-overexpressing TNBC cells and may identify new therapeutic targets for this clinically challenging subset of breast cancer. Using a targeted metabolomics approach, we identified fatty acid oxidation (FAO) intermediates as being dramatically upregulated in a MYC-driven model of TNBC. We also identified a lipid metabolism gene signature in patients with TNBC that were identified from The Cancer Genome Atlas database and from multiple other clinical data sets, implicating FAO as a dysregulated pathway that is critical for TNBC cell metabolism. We found that pharmacologic inhibition of FAO catastrophically decreased energy metabolism in MYC-overexpressing TNBC cells and blocked tumor growth in a MYC-driven transgenic TNBC model and in a MYC-overexpressing TNBC patient–derived xenograft. These findings demonstrate that MYC-overexpressing TNBC shows an increased bioenergetic reliance on FAO and identify the inhibition of FAO as a potential therapeutic strategy for this subset of breast cancer.

We hypothesized that MYC-dependent metabolic dysregulation is essential for MYC-overexpressing TNBC. To test this hypothesis, we investigated tumor metabolism in a conditional doxycycline-inducible transgenic model of MYC-overexpressing TNBC (MTB-TOM)[5,6]. We used mass spectrometry to compare the global metabolic profile of MTB-TOM tumors to that of naive mammary glands from MTB-TOM transgenic mice in which MYC was not induced. Metabolite analysis revealed a number of dysregulated pathways in MTB-TOM tumors that are commonly associated with tumorigenesis—including glycolysis, the tricarboxylic acid (TCA) cycle and fatty acid metabolism (**Fig. 1a**, **Supplementary Fig. 1** and **Supplementary Table 1**). Although fatty acid synthesis (FAS) is upregulated in many types of cancer, a MYC-dependent role for FAO in breast tumorigenesis has not previously been described[4,7,8]. Considering the proximity of primary breast tumors to the adipose-rich mammary gland, we chose to focus on the dysregulation of FAO in MYC-overexpressing TNBC cells.

To investigate the role of MYC in FAO upregulation in TNBC cells, we returned to our MTB-TOM metabolomic data (**Supplementary Table 1**). Acylcarnitines are an essential intermediate and are involved in the first committed step of FAO[9]. To catabolize long-chain fatty acids (such as palmitate) to acetyl–coenzyme A (acetyl-CoA), a major fuel for biosynthetic and bioenergetic metabolism, acyl-CoAs must be enzymatically converted to acylcarnitines across the outer mitochondrial membrane by carnitine palmitoyltransferase 1 (CPT1A or CPT1B)[9]. We found that all six acylcarnitine intermediates detected in our metabolomic analysis were significantly elevated in MTB-TOM tumors than in control tissue (**Fig. 1b**). To further validate these steady-state findings *in vivo*, we assayed acylcarnitine production in MTB-TOM tumors 4 h after intraperitoneal (i.p.) injection of [^{13}C]palmitate into tumor-bearing mice. Tumor tissue had a fourfold increase in [^{13}C]palmitoyl-carnitine production, as compared to that in control mammary gland tissue (**Fig. 1c**). Because [^{13}C]palmitoyl-carnitine production was not normalized to overall uptake in this experiment, this increase could reflect a relative increase in fatty acid uptake, fatty acid utilization via oxidation or both. Nevertheless, taken together, these data indicate that the first committed step of FAO is upregulated in MYC-overexpressing TNBC cells.

To determine how FAO is altered in TNBC, we analyzed RNA expression data from primary human tumors (771 patient samples from The

[1]Department of Cell and Tissue Biology, University of California, San Francisco (UCSF), San Francisco, California, USA. [2]Biomedical Sciences Graduate Program, University of California, San Francisco, San Francisco, California, USA. [3]Program in Metabolic Biology, University of California, Berkeley, Berkeley, California, USA. [4]Diabetes Center, University of California, San Francisco, San Francisco, California, USA. [5]Eli and Edythe Broad Center of Regeneration Medicine and Stem Cell Research, University of California, San Francisco, San Francisco, California, USA. [6]Department of Otolaryngology, University of California, San Francisco, San Francisco, California, USA. [7]Department of Pathology, University of California, San Francisco, San Francisco, California, USA. [8]Department of Medicine, University of California, San Francisco, San Francisco, California, USA. [9]Helen Diller Family Comprehensive Cancer Center, University of California, San Francisco, San Francisco, California, USA. Correspondence should be addressed to A.G. (andrei.goga@ucsf.edu).

Received 16 November 2015; accepted 3 February 2016; published online 7 March 2016; doi:10.1038/nm.4055

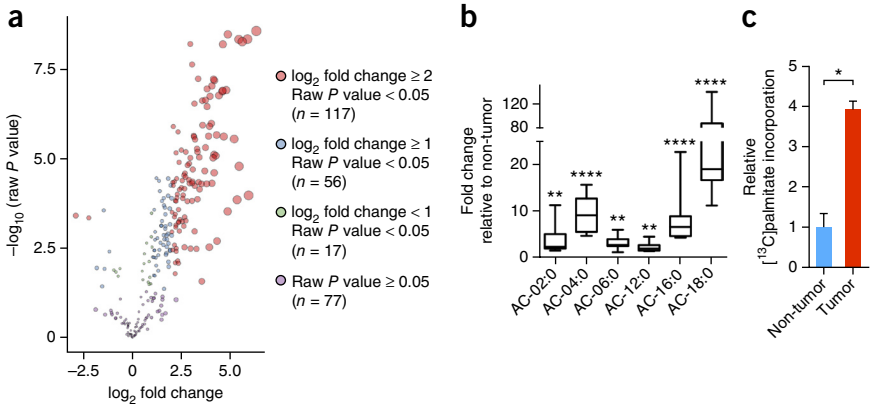

Figure 1 MTB-TOM tumors show dysregulated FAO. (**a**) Volcano plot for changes in metabolite concentrations in MTB-TOM tumors (seven tumors from five induced mice) as compared to those from non-tumor mammary glands (five mammary glands from four uninduced mice). (**b**) Fold change in acylcarnitine (AC) levels in MTB-TOM tumors versus non-tumor mammary glands, in the same mice as in **a**. Values are shown as minimum-to-maximum box plots. Error bars indicate range of smallest to largest value recorded. The *x* axis designations indicate acyl-carbon chain length followed by the location of any double bonds (e.g., 'AC-02:0' indicates a two-carbon acyl group with no double bonds). (**c**) [^{13}C]palmitoyl-carnitine production from [^{13}C]palmitate, as assessed by carbon flux analysis, in MTB-TOM orthotopic transplants, as compared to that in the contralateral non-tumor mammary gland in the same mouse ($n = 4$ mice). Throughout, the values shown are mean ± s.e.m. In **c**, a two-tailed unpaired *t*-test was used to compare non-tumor to tumor samples. In **a**,**b**, all differential metabolite-abundance analyses were performed using the 'limma' R package. $^{*}P < 0.05$, $^{**}P < 0.01$, $^{****}P < 0.0001$.

Cancer Genome Atlas (TCGA)). Of 336 genes associated with fatty acid metabolism in the Gene Ontology database (GO:0006631), we found that 244 (73%) were significantly dysregulated (false-discovery rate (FDR) < 0.05) in triple-negative (TN) versus RP breast tumors (**Supplementary Table 2**). We also found that TN tumors showed upregulation of many genes that encode activators of FAO (including the gene encoding the master transcriptional regulator PPARG coactivator 1 alpha (also known as PGC-1α; encoded by *PPARGC1A*)) and downregulation of many genes that encode activators of fatty acid synthesis (FAS) (including fatty acid synthase (*FASN*) and acetyl-coA carboxylase beta (*ACACB*; also known as *ACC2*)) (**Supplementary Table 2**). We applied the fatty acid metabolism signature identified from TCGA samples (**Fig. 2a**) to four additional breast cancer clinical cohorts (2,119 total patients including those from TCGA) and confirmed that this signature was highly correlated with TNBC tumor samples (**Supplementary Fig. 2** and **Supplementary Table 3**)[10–13]. Next we confirmed upregulation of key FAO activators and downregulation of key FAS activators at the protein level in TN versus RP

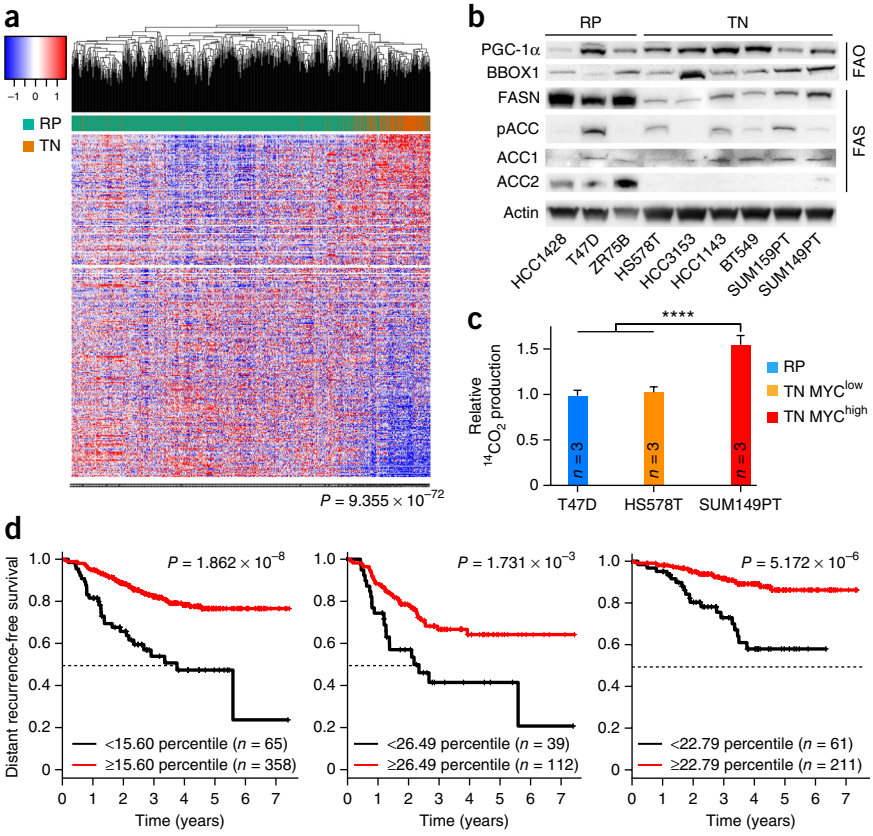

Figure 2 Human TNBC shows dysregulated FAO. (**a**) Hierarchical clustering of TCGA RNA-seq samples from 771 breast cancer patients for 336 fatty acid metabolism genes in TN and RP tumors. Individual gene expression is row-normalized from −1 (blue) to 1 (red). A Fisher's exact test was used to calculate the indicated *P* value, which demonstrated significant enrichment of genes in the clade indicated by a red box in TN tumors (116/123). (**b**) Immunoblot analysis showing expression levels of FAO activators PGC-1α and BBOX1 and of fatty acid synthesis enzymes FASN, ACC1, ACC2, and phosphorylated ACC1 and ACC2 (pACC) in a panel of TN and RP human cell lines (RP lines, $n = 3$; TN lines, $n = 6$). (**c**) Quantification of FAO assays in TN MYC^{high}, TN MYC^{low} and RP cells. Relative $^{14}CO_2$ production was normalized for each cell line to total protein levels. Values shown are mean ± s.e.m. A two-tailed unpaired *t*-test was used to compare non-tumor to tumor samples. $^{****}P < 0.0001$. (**d**) Kaplan-Meier survival graphs for all patients with tumors (left) or for those with TN (middle) or RP (right) tumors, from a pooled neoadjuvant chemotherapy–treated cohort and grouped on the basis of *ACACB* (*ACC2*) mRNA expression at an optimal threshold indicated by percentile numbers. Samples with decreased *ACACB* expression are represented with black lines. Median survival times (MSTs) are indicated by the black dashed lines. For all tumors, *ACACB*^{low} MST = 3.76 years; for TN tumors, *ACACB*^{low} MST = 2.18 years; the MST was not reached in any other group. A log-rank test was used to calculate *P* values. In **a**, differential gene expression analyses were performed using the limma R package.

© 2016 Nature America, Inc. All rights reserved.

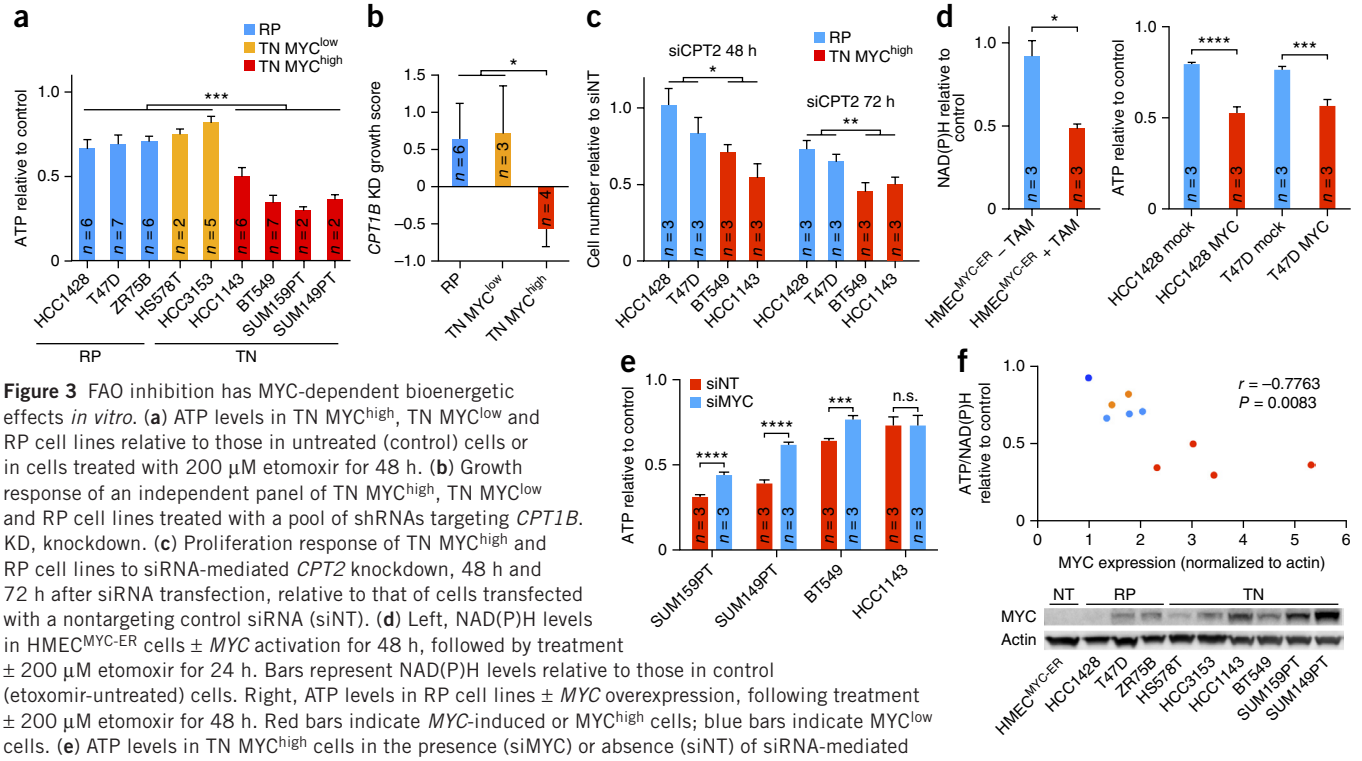

Figure 3 FAO inhibition has MYC-dependent bioenergetic effects *in vitro*. (**a**) ATP levels in TN MYC^{high}, TN MYC^{low} and RP cell lines relative to those in untreated (control) cells or in cells treated with 200 μM etomoxir for 48 h. (**b**) Growth response of an independent panel of TN MYC^{high}, TN MYC^{low} and RP cell lines treated with a pool of shRNAs targeting *CPT1B*. KD, knockdown. (**c**) Proliferation response of TN MYC^{high} and RP cell lines to siRNA-mediated *CPT2* knockdown, 48 h and 72 h after siRNA transfection, relative to that of cells transfected with a nontargeting control siRNA (siNT). (**d**) Left, NAD(P)H levels in HMEC$^{MYC\text{-}ER}$ cells ± *MYC* activation for 48 h, followed by treatment ± 200 μM etomoxir for 24 h. Bars represent NAD(P)H levels relative to those in control (etoxomir-untreated) cells. Right, ATP levels in RP cell lines ± *MYC* overexpression, following treatment ± 200 μM etomoxir for 48 h. Red bars indicate *MYC*-induced or MYC^{high} cells; blue bars indicate MYC^{low} cells. (**e**) ATP levels in TN MYC^{high} cells in the presence (siMYC) or absence (siNT) of siRNA-mediated *MYC* knockdown ± treatment with 200 μM etomoxir for 48 h. Bars represent ATP levels relative to those in control (etoxomir-untreated) cells. (**f**) Top, correlation of MYC protein expression and mean ATP/NAD(P)H response to etomoxir treatment in TN and RP cell lines in **a** and in HMEC$^{MYC\text{-}ER}$ cells without MYC in **b**. Pearson correlation and two-tailed *t*-test were used to generate the correlation coefficient and associated *P* value. The color code is the same as in **a**, except that HMEC$^{MYC\text{-}ER}$ cells are indicated in dark blue. Bottom, immunoblot analysis showing MYC protein levels in the indicated cell lines. Throughout, values shown are mean ± s.e.m. from triplicate samples (**a**,**d**,**e**), the indicated number of cell lines (**b**) or three biological replicates (**c**). The number of biological replicates is indicated (**a**,**c**–**e**). A two-tailed unpaired *t*-test was used to compare experimental groups (**a**–**e**); $^{*}P \le 0.05$, $^{**}P < 0.01$, $^{***}P < 0.001$, $^{****}P < 0.0001$.

human breast cancer cell lines (**Fig. 2b**)[4,14,15]. Notably, whereas FASN and ACC2 were markedly downregulated in TN cell lines as compared to RP cells, ACACA (ACC1) was expressed equivalently in TN and RP cell lines. To directly test whether FAO is increased in MYC^{high} TNBC cells, we measured [^{14}C]oleic acid conversion to $^{14}CO_2$ and found an ~50% increase in FAO in MYC^{high} TNBC cells as compared to MYC^{low} TNBC cells or to RP cells (**Fig. 2c**). Taken together, these data suggest that FAO is upregulated in MYC^{high} TNBC cells.

TNBC is the most aggressive subtype of breast cancer and is characterized by poor clinical outcome[1,2]. To determine whether FAO gene expression is associated with prognosis, we performed univariate analysis of the 336 fatty acid metabolism genes on a patient cohort with long-term distant recurrence-free survival data (**Supplementary Table 4**)[11]. We found that decreased expression of *ACACB*—which encodes the ACC2 enzyme that produces malonyl-CoA to directly inhibit CPT1A and CPT1B, and therefore FAO—was associated with worse prognosis for all patients, as well as for the TNBC cohort (**Fig. 2d**)[9]. Although decreased *ACACB* expression was also associated with worse outcome for patients with RP tumors, the median time to distant recurrence-free survival was not reached in this cohort, suggesting that FAO may be a less important marker of tumor recurrence in RP cancers (**Fig. 2d**). These patient data suggest that decreased *ACACB* expression, and thus increased FAO, may contribute to the aggressiveness of breast tumors, with the worst outcome occurring in the TNBC subset.

FAO is the primary bioenergetic pathway in many non-tumor tissues[9]. We therefore investigated whether this pathway is essential for energy production in MYC-overexpressing TNBC. We used etomoxir (a clinically tested, specific inhibitor of CPT1)[16] to determine the effects of FAO inhibition on ATP and NAD(P)H production. We first examined nine human breast cancer cell lines (six TN and three RP) with various levels of MYC expression[15]. Etomoxir treatment dramatically inhibited ATP production in TNBC cell lines expressing high amounts of MYC, whereas TN and RP cell lines expressing low amounts of MYC were significantly less affected (**Fig. 3**). Analysis of cell proliferation and apoptosis revealed that etomoxir-treated MYC^{high} cells show decreased proliferation without a decrease in viability (**Supplementary Fig. 3** and **Supplementary Data**).

To validate the requirement for FAO in MYC-overexpressing TNBC, we used an orthogonal approach in which we extracted data from the Project Achilles data set[17] for the knockdown of *CPT1B*. Specifically, the growth of 216 cancer cell lines was measured after each line was treated independently with five shRNAs specific for *CPT1B*[17]. To determine whether *CPT1B* expression was required for breast cancer growth, we focused on the 13 breast cancer cell lines tested (of which there was no overlap with the lines used above): BT20, CAL120, CAL51, HCC1187, HCC1395, HCC70, MDAMB453, BT474, EFM19, HCC1954, HCC2218, MCF7 and ZR7530. We categorized these lines as RP, TN MYC^{low} and TN MYC^{high} (as in **Fig. 3a**) on the basis of *MYC* expression levels (data not shown). We found that the growth of TN MYC^{high} cells was significantly more sensitive to *CPT1B* knockdown than that of RP or TN MYC^{low} cells (**Fig. 3b**). Additionally, we used siRNA to deplete *CPT2*, which encodes another essential FAO enzyme[9]. *CPT2* knockdown markedly decreased proliferation

© 2016 Nature America, Inc. All rights reserved.

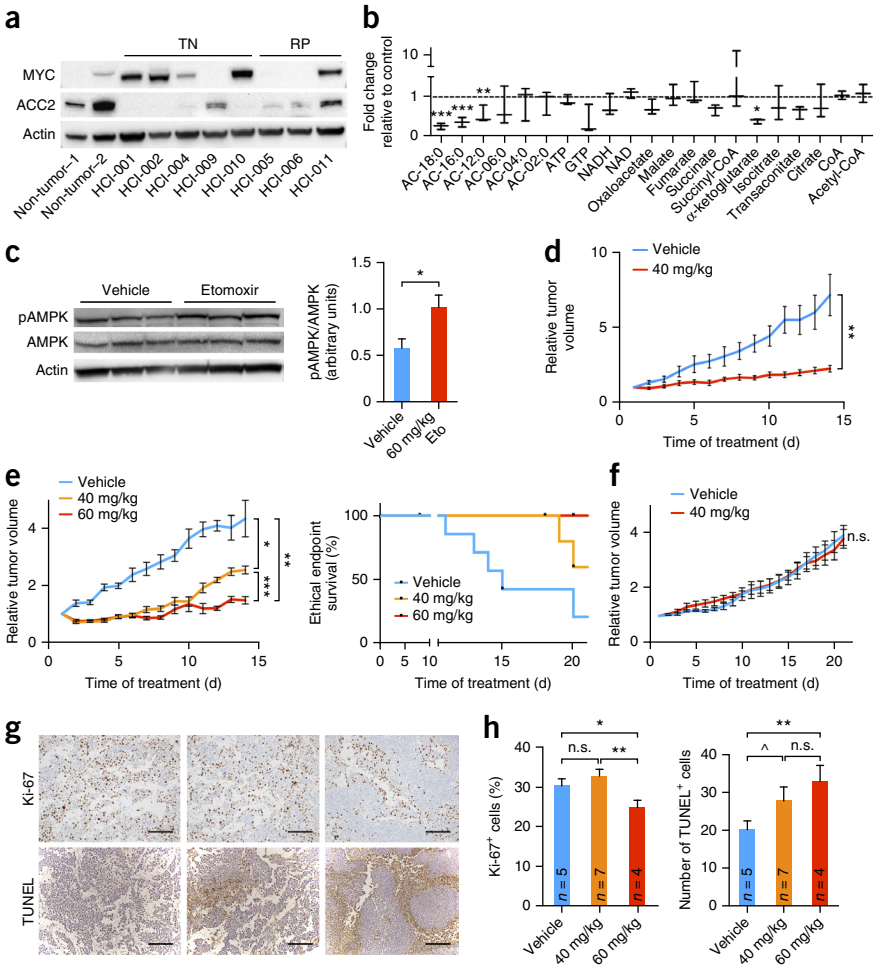

Figure 4 FAO inhibition has MYC-dependent bioenergetic and growth effects *in vivo*. (**a**) Immunoblot analysis of MYC and ACC2 protein expression in patient-derived xenografts from individuals with TN ($n = 5$) or RP ($n = 3$) tumors, as well as in human non-tumor reduction mammoplasty tissues (non-tumor–1 and non-tumor–2). (**b**) Fold change in metabolite levels in etomoxir-treated xenograft tumors (HCI-002) versus vehicle-treated tumors. Values are shown as minimum-to-maximum box plots for three mice in each group. (**c**) Left, immunoblot analysis of pAMPK and AMPK expression in etomoxir- or vehicle-treated HCI-002 tumors ($n = 3$ mice). Right, quantitation of the pAMPK/AMPK ratio, normalized to β-actin levels. Eto, etomoxir. (**d**) Relative tumor volume of orthotopic MTB-TOM (MYC^{high}) tumor allografts in FVB/N mice that were treated with vehicle ($n = 6$ mice) or etomoxir (40 mg/kg; $n = 7$ mice) daily for 14 d. (**e**) Left, relative tumor volume of orthotopic HCI-002 (MYC^{high}) xenografts in NOD/SCID mice that were treated with vehicle ($n = 7$) or with 40 mg/kg ($n = 5$) or 60 mg/kg ($n = 5$) etomoxir daily for 21 d. Right, Kaplan-Meier analysis of mice with HCI-002 xenografts that were treated with vehicle ($n = 7$) or with 40 mg/kg ($n = 5$) or 60 mg/kg ($n = 5$) etomoxir. Ethical endpoint survival indicates the percentage of mice bearing xenografts <2 cm in size. $P = 0.0045$ by log-rank test. (**f**) Relative tumor volume of orthotopic HCI-009 (MYC^{low}) xenografts in NOD/SCID mice that were treated with vehicle or etomoxir (40 mg/kg) daily for 21 d ($n = 3$ mice per group). (**g**,**h**) Representative (of three high-powered (20×) fields from two separate areas of each tumor) Ki-67 (top) and TUNEL (bottom) staining of HCI-002 tumors in mice (killed at the end of the study) that were treated with vehicle (left) or with 40 mg/kg (middle) or 60 mg/kg (right) etomoxir (**g**) and quantification of $Ki\text{-}67^+$ cells/field (**h**, left) and $TUNEL^+$ cells/field (**h**, right). The number of mice analyzed in each treatment group is indicated in **h**. Scale bars, 200 μm. In **b**, all differential metabolite abundance analyses were performed using the limma R package. Unless otherwise specified, values shown are mean ± s.e.m. In **d**–**f**, tumor volume is shown relative to tumor volume on day 1 of treatment. A two-tailed unpaired *t*-test was used to compare experimental groups (**c**–**g**); $^{\wedge}P \leq 0.10$, $^{*}P \leq 0.05$, $^{**}P < 0.01$, $^{***}P < 0.001$; n.s., not significant.

© 2016 Nature America, Inc. All rights reserved.

of MYC^{high} TN cells, but it had a significantly weaker growth inhibitory effect on RP cells (**Fig. 3c** and **Supplementary Fig. 4**). Thus, the results obtained with small-molecule inhibition or with knockdown of *CPT1B*, as well as with knockdown of *CPT2*, suggest that FAO is an essential metabolic pathway in MYC-overexpressing TNBC cells.

FAO has been shown to be important for cells that have become detached from matrix and that are grown in nutrient-deprived conditions[18,19]. We therefore asked whether TN receptor and MYC status affect the response to FAO inhibition for tumor cells that are either not attached to matrix or deprived of glucose. To model matrix detachment, we used ultra-low-adhesion plates and grew breast cancer cell lines as spheres. Whereas TN MYC^{high}, TN MYC^{low} and RP cells were all able to form viable spheres upon matrix detachment, TN MYC^{high} cells were significantly ($P < 0.0001$) more sensitive to FAO inhibition (**Supplementary Fig. 5**). Next we tested the additive effect of FAO inhibition and glucose deprivation. Both TN MYC^{high} and TN MYC^{low} cells showed an increased sensitivity to glucose deprivation, as compared to that for RP cells (**Supplementary Fig. 6**), consistent with the well-established dependence on glycolysis for TNBC cell growth[20]. Concurrent depletion of glucose and inhibition of FAO resulted in an additive effect on ATP depletion in TN, but not in RP, cells (**Supplementary Fig. 6**). These results are consistent with previous findings that FAO is important for breast cancer cell survival and NADPH production, for conditions of limited glycolysis[21], and suggest that TN MYC^{high} cells are more reliant on FAO for survival than MYC^{low} cells under conditions of matrix detachment or nutrient deprivation.

To confirm that the observed bioenergetic reliance for FAO in MYC-overexpressing TNBC cells is a MYC-dependent phenotype, we examined whether conditional *MYC* expression alters the sensitivity of cells to FAO inhibition. We used two approaches; the first was to use non-tumor human mammary epithelial (HMEC) cells expressing a 4-hydroxytamoxifen (TAM)-inducible MYC–estrogen receptor (ER) fusion protein (hereafter referred to as $HMEC^{MYC\text{-}ER}$ cells), and the second was to use two RP lines, each stably transduced with a *MYC* overexpression construct or control vector[1,15] (**Supplementary Fig. 7**). TAM-induced $HMEC^{MYC\text{-}ER}$ and *MYC*-transduced RP cells were significantly more sensitive to etomoxir than uninduced $HMEC^{MYC\text{-}ER}$ and vector-transduced RP cells, respectively (**Fig. 3d**). Furthermore, siRNA-mediated knockdown of *MYC* significantly rescued etomoxir sensitivity in three of four MYC^{high} TNBC cell lines tested (**Fig. 3e** and **Supplementary Fig. 8**). Finally, MYC protein expression significantly

correlated with bioenergetic sensitivity to FAO inhibition in our panel of human breast cancer cell lines (**Fig. 3f**). Although MYC expression was not tightly correlated with FAO or FAS protein expression (**Figs. 2b** and **3f**), it did correlate well with FAO-inhibition sensitivity and FAO activity (**Figs. 2c** and **3f**). These data suggest that *MYC* expression is both necessary and sufficient to induce a bioenergetic reliance for FAO in breast epithelial and breast cancer cells.

Given that our initial observation of dysregulated FAO was made in MYC-driven breast tumors, we sought to test the effects of FAO inhibition on the metabolism of MYC-overexpressing TNBC *in vivo*. We obtained a panel of human TN and RP breast cancer patient–derived xenografts (PDX) with various MYC levels (**Fig. 4a**)[22]. We administered etomoxir (60 mg per kg of body weight (mg/kg)) or vehicle by i.p. injection to mice bearing orthotopic HCI-002 MYC^{high} TNBC PDXs at two time points (0 and 24 h) (**Fig. 4a**)[22]. Metabolite analysis of HCI-002 tumors harvested at 26 h revealed a significant reduction in long-chain acylcarnitine levels, as well as a reduction in TCA cycle intermediates (especially α-ketoglutarate) in drug-treated tumors, as compared to vehicle-treated tumors (**Fig. 4b** and **Supplementary Table 5**). Etomoxir-treated tumors had a significant increase in phosphorylated AMPK (pAMPK) levels, a well-established marker of bioenergetic stress, as compared to control-treated tumors (**Fig. 4c**). In a second metabolomic study, as compared to vehicle-treated tumors, MTB-TOM tumors that were treated with 20 mg/kg etoxomir for 14 d showed a marked reduction in the levels of the majority of TCA cycle intermediates measured, as well as in the level of ATP, and also showed a significant ($P < 0.05$) increase in AMP/ATP, ADP/ATP, UMP/UTP and UDP/UTP ratios (**Supplementary Fig. 9** and **Supplementary Table 6**). These data indicate that treatment with an FAO inhibitor decreases bioenergetic metabolism *in vivo* in both transgenic and PDX models of TNBC.

This observed reduction in bioenergetic metabolism prompted us to analyze the effects of prolonged FAO inhibition on the growth of MYC-overexpressing TNBC tumors. We performed orthotopic transfer of MTB-TOM or HCI-002 PDX tumors into the mammary fat pad of syngeneic FVB/N or immunodeficient NOD/SCID mice, respectively. In the case of MTB-TOM allograft-bearing mice, we administered 40 mg/kg etomoxir or vehicle by i.p. injection daily for 14 d; in the case of HCI-002 PDX–bearing mice, we administered 40 or 60 mg/kg etomoxir or vehicle by i.p. injection daily for 21 d. Etomoxir treatment resulted in a significant attenuation of tumor growth in both models and a significant extension of the time to ethical end point in the PDX model (**Fig. 4d**,**e**). In contrast, we observed no significant attenuation in tumor growth of mice with HCI-009 MYC^{low} TNBC PDX tumors that were treated with 40 mg/kg etomoxir (**Fig. 4f**). HCI-009 showed a moderate level of ACC2 expression (**Fig. 4a**), suggesting that FAO might be attenuated in these tumors and explaining their resistance to etomoxir. The efficacy of etoxomir in both MYC^{high} transgenic and PDX models, but not in a MYC^{low} PDX model, suggests that high MYC expression, as well as low ACC2 expression, may serve as a biomarker of sensitivity to FAO inhibition.

Next we determined the effects of FAO inhibition on cell proliferation and death. HCI-002 PDX–bearing mice that were treated with 60 mg/kg etomoxir showed significantly decreased staining of the cell proliferation marker Ki-67 in the tumors (indicative of decreased cell proliferation), as compared to tumors from vehicle-treated mice, and a dose-dependent increase in TUNEL staining (indicative of increased apoptosis) (**Fig. 4g**,**h**). In contrast, etomoxir treatment of cultured MYC-overexpressing TNBC cell lines had a marked effect on cell proliferation but no appreciable effects on cell death (**Supplementary Fig. 3**). These contrasting results suggest that FAO has a more critical role for *in vivo* tumor cell viability than it does *in vitro*.

Elevated MYC expression was recently discovered to be a defining factor of TNBC[1,2]. The present study is among the first to investigate the role of MYC in TNBC metabolism *in vivo*[20]. Here we show that FAO is upregulated in MYC-overexpressing TNBC cells and that TNBC is sensitive to FAO inhibition in a MYC-dependent manner, as shown using several models of MYC-overexpressing TNBC *in vitro* and PDX and transgenic models *in vivo*. This work supports a critical role for FAO in TNBC, and it identifies high levels of MYC expression as a marker for this dependence. On the basis of our findings, inhibition of FAO as a therapeutic strategy for MYC-overexpressing TNBC should be further investigated.

METHODS

Methods and any associated references are available in the online version of the paper.

Note: Any Supplementary Information and Source Data files are available in the online version of the paper.

ACKNOWLEDGMENTS

This work was supported, in part, by the US Department of Defense–Congressionally Directed Medical Research Programs' Era of Hope Scholar award W81XWH-12-1-0272 (A.G.), the US National Institutes of Health (NIH) grant R01 CA170447 (A.G.), the Diabetes, Endocrinology and Metabolism training grant T32 DK007418 (R.C.), the Molecular and Cellular Mechanisms of Cancer training grant T32 CA108462 (A.Y.Z.) and the Atwater Foundation (A.G.). The authors thank A. Welm for guidance in the use of patient-derived xenografts, D. Lowe and A. Beardsley for technical guidance and helpful discussions, K.A. Fontaine for helpful discussions and comments on the manuscript, and S. Samson for a helpful consumer advocate perspective and guidance on our work.

AUTHOR CONTRIBUTIONS

R.C. designed and conducted all of the experiments, except the initial MTB-TOM metabolomic and $HMEC^{MYC\text{-}ER}$ studies, and wrote the manuscript. A.Y.Z. performed the *in vivo* studies and provided intellectual input and valuable discussion. R.A.K. performed the mass spectrometry and metabolomic analyses. S.B. performed bioinformatic analyses of the data from the gene expression and metabolomic analyses. C.M. performed the *in vitro* proliferation and viability studies, did the matrix detachment studies and assisted in TUNEL quantification. B.A. performed the $HMEC^{MYC\text{-}ER}$ studies and provided valuable discussion. H.E. performed the orthotopic tumor transplants. S.K. supervised the FAO activity analyses. A.T. provided the *CPT1B*-knockdown data, interpreted data and was provided valuable discussion. G.K. constructed the HCI-002 etomoxir study tissue microarray and performed Ki-67 staining and quantification. D.K.N. supervised the mass spectrometry and metabolomic analyses, and provided valuable discussion. A.G. supervised all of the studies, and provided valuable discussion and intellectual input. All authors edited the manuscript.

COMPETING FINANCIAL INTERESTS

The authors declare no competing financial interests.

Reprints and permissions information is available online at http://www.nature.com/reprints/index.html.

1. Horiuchi, D. *et al.* MYC pathway activation in triple-negative breast cancer is synthetic lethal with CDK inhibition. *J. Exp. Med.* **209**, 679–696 (2012).
2. Koboldt, D.C. *et al.* Comprehensive molecular portraits of human breast tumors. *Nature* **490**, 61–70 (2012).
3. Hu, S. *et al.* [^{13}C]pyruvate imaging reveals alterations in glycolysis that precede c-Myc–induced tumor formation and regression. *Cell Metab.* **14**, 131–142 (2011).
4. Wahlström, T. & Henriksson, M.A. Impact of MYC in regulation of tumor cell metabolism. *Biochim. Biophys. Acta* **1849**, 563–569 (2015).
5. D'Cruz, C.M. *et al.* c-MYC induces mammary tumorigenesis by means of a preferred pathway involving spontaneous *Kras2* mutations. *Nat. Med.* **7**, 235–239 (2001).
6. Pfefferle, A.D. *et al.* Transcriptomic classification of genetically engineered mouse models of breast cancer identifies human subtype counterparts. *Genome Biol.* **14**, R125 (2013).
7. Carracedo, A. *et al.* A metabolic prosurvival role for PML in breast cancer. *J. Clin. Invest.* **122**, 3088–3100 (2012).

© 2016 Nature America, Inc. All rights reserved.

8. Zaugg, K. *et al.* Carnitine palmitoyltransferase 1C promotes cell survival and tumor growth under conditions of metabolic stress. *Genes Dev.* **25**, 1041–1051 (2011).
9. Bonnefont, J.P. *et al.* Carnitine palmitoyltransferases 1 and 2: biochemical, molecular and medical aspects. *Mol. Aspects Med.* **25**, 495–520 (2004).
10. Esserman, L.J. *et al.* Chemotherapy response and recurrence-free survival in neoadjuvant breast cancer depends on biomarker profiles: results from the I-SPY 1 TRIAL (CALGB 150007/150012; ACRIN 6657). *Breast Cancer Res. Treat.* **132**, 1049–1062 (2012).
11. Hatzis, C. *et al.* A genomic predictor of response and survival following taxane-anthracycline chemotherapy for invasive breast cancer. *JAMA* **305**, 1873–1881 (2011).
12. Yau, C. *et al.* A multigene predictor of metastatic outcome in early-stage hormone receptor–negative and triple-negative breast cancer. *Breast Cancer Res.* **12**, R85 (2010).
13. Chin, K. *et al.* Genomic and transcriptional aberrations linked to breast cancer pathophysiologies. *Cancer Cell* **10**, 529–541 (2006).
14. Morris, E.M. *et al.* PGC-1α overexpression results in increased hepatic fatty acid oxidation with reduced triacylglycerol accumulation and secretion. *Am. J. Physiol. Gastrointest. Liver Physiol.* **303**, G979–G992 (2012).
15. Neve, R.M. *et al.* A collection of breast cancer cell lines for the study of functionally distinct cancer subtypes. *Cancer Cell* **10**, 515–527 (2006).
16. Holubarsch, C.J.F. *et al.* A double-blind randomized multicenter clinical trial to evaluate the efficacy and safety of two doses of etomoxir, in comparison with placebo, in patients with moderate congestive heart failure: the ERGO (etomoxir for the recovery of glucose oxidation) study. *Clin. Sci.* **113**, 205–212 (2007).
17. Cowley, G.S. *et al.* Parallel genome-scale loss-of-function screens in 216 cancer cell lines for the identification of context-specific genetic dependencies. *Sci. Data* **1**, 140035 (2014).
18. Jeon, S.M., Chandel, N.S. & Hay, N. AMPK regulates NADPH homeostasis to promote tumor cell survival during energy stress. *Nature* **485**, 661–665 (2012).
19. Schafer, Z.T. *et al.* Antioxidant and oncogene rescue of metabolic defects caused by loss of matrix attachment. *Nature* **461**, 109–113 (2009).
20. Shen, L. *et al.* Metabolic reprogramming in triple-negative breast cancer through Myc suppression of TXNIP. *Proc. Natl. Acad. Sci. USA* **112**, 5425–5430 (2015).
21. Bensaad, K. *et al.* Fatty acid uptake and lipid storage induced by HIF-1α contribute to cell growth and survival after hypoxia-reoxygenation. *Cell Rep.* **9**, 349–365 (2014).
22. DeRose, Y.S. *et al.* Tumor grafts derived from women with breast cancer authentically reflect tumor pathology, growth, metastasis and disease outcomes. *Nat. Med.* **17**, 1514–1520 (2011).

© 2016 Nature America, Inc. All rights reserved.

ONLINE METHODS

Patient-derived xenograft models. All human samples used to generate PDX tumors, as well as the human non-tumor samples, were previously described[22].

MTB-TOM tumor generation. All protocols described in this and other sections regarding animal studies were approved by the UCSF Institutional Animal Care and Use Committee. MTB-TOM (MMTV-rtTA/TetO-*MYC*) mice were generated as previously described[5]. Mice were bred and maintained off of doxycycline. At 12–15 weeks of age, female mice were put on doxycycline (200 mg/kg doxy chow, Bio-Serv) to induce *MYC* expression and tumorigenesis. Mice were monitored daily for tumor growth by inspection and caliper measurement in two dimensions. Mice were sacrificed as per ethical guidelines (tumors reaching 2 cm in any single dimension) and tumor(s) or mammary gland(s) were flash-frozen in liquid nitrogen.

Metabolomics. For U-[^{13}C]palmitate flux analyses, the labeled palmitate (Cambridge Isotope Laboratories Inc., CLM-409-0.5) or unlabeled palmitate (Sigma) was diluted in PEG40 (Spectrum) via sonication and was administered via intraperitoneal injection at 100 mg/kg. 4 h after the injection, the animals were sacrificed and the tumors were flash-frozen.

Nonpolar metabolites were extracted using a Dounce homogenizer in 4 ml of 2:1:1 chloroform:methanol:PBS spiked with 10 nmol of internal standards (C12:0 dodecylglycerol and pentadecanoic acid; Sigma). Separation of organic and aqueous layers was achieved via centrifugation at 1,000*g* for 5 min at 4 °C. Secondary extraction of the aqueous layer was performed using 0.1% formic acid followed by addition of 2 ml chloroform and further centrifugation. After combining the organic extractions, the lipid-containing mixture was dried under nitrogen (N_2) and dissolved in 120 µl chloroform. Single-reaction monitoring (SRM) liquid chromatography–coupled to tandem mass spectrometry (LC-MS/MS)—on an Agilent 6400 series QQQ using 10 µl of sample—was achieved using a reverse-phase C5 column (Phenomenex, Luna 50 mm × 4.6 mm, 5-µm particle diameter). Mobile phases were buffer A (composed of 95:5 water:methanol) and buffer B (60:35:5 2-propanol:methanol:water). Solvent modifiers were 0.1% formic acid with 5 mM ammonium formate or 0.1% ammonium hydroxide for positive and negative ionization modes, respectively.

For polar metabolites, frozen tissue was homogenized using a TissueLyser in 300 µl of 40:40:20 acetonitrile:methanol:water with the addition of 1 nM (final concentration) of D3-[^{15}N]serine as an internal extraction standard (Cambridge Isotopes Laboratories Inc, DNLM-6863). 10 µl of cleared supernatant (via centrifugation at 15,000 r.p.m., 10 min, at 4 °C) was used for SRM–LC-MS/MS using a normal-phase Luna NH_2 column (Phenomenex). Mobile phases were buffer A (composed of 100% acetonitrile) and buffer B (composed of 95:5 water:acetonitrile). Solvent modifiers were 0.1% formic acid or 0.2% ammonium hydroxide with 50 mM ammonium acetate for positive and negative ionization modes, respectively.

All metabolites were analyzed using the MassHunter software package (Agilent Technologies) by quantifying the transition from parent precursor mass to product ions for each individual metabolite.

Gene expression analysis. TCGA breast-invasive carcinoma data set was sourced from data generated by TCGA Research Network (http://cancergenome.nih.gov), made available on the University of California, Santa Cruz (UCSC) Cancer Browser. Series matrix files for ISPY1 (accession code GSE22226) and a neoadjuvant chemotherapy–treated cohort (accession code GSE25066) were downloaded from the Gene Expression Omnibus (GEO) site and processed using the GEOquery R package[10,11,23]. A chemotherapy-naive cohort and an aggressively treated early-stage cohort were obtained from the UCSC Cancer Browser[12,13]. Multiple probes corresponding to the same gene were collapsed using the 'MaxMean' method in the weighted correlation network analysis (WGCNA) R package[24,25].

A fatty acid metabolism gene set was compiled using genes containing the Gene Ontology term, GO:0006631 (http://geneontology.org). An average expression profile (centroid) of these genes was calculated for the triple-negative subset of samples within the breast-invasive carcinoma data set from TCGA. Similarities between this centroid and the gene expression profiles of samples from the four independent clinical cohorts were then quantified using a Pearson correlation metric.

Heat maps and clustering analyses were performed using the 'gplots' (http://cran.r-project.org/web/packages/gplots/index.html) and 'cluster' (http://cran.r-project.org/web/packages/cluster/index.html) R packages respectively.

To generate Kaplan-Meier plots, samples were grouped by receptor status and dichotomized by *ACC2* expression at an optimal threshold, yielding groups with the most significant difference in distant recurrence-free survival based on the log-rank test. Kaplan-Meier plots were then generated for the respective groups using the 'survival' (http://cran.r-project.org/web/packages/survival/index.html) R package.

Univariate Cox proportional-hazards regression analysis was performed using the 'survival' R package to assess the correlation of fatty acid metabolism gene expression to distant recurrence-free survival in the pooled neoadjuvant chemotherapy–treated cohort[11]. This was conducted for all tumors, TN tumors and RP tumors.

Cell lines and propagation. A panel of established TN and RP human breast cancer cell lines, and their culture conditions, have previously been described[15]. Primary human mammary epithelial (HMEC) cells were derived from histologically normal breast tissues and cultured as previously described[26]. The cells were infected with a lentivirus expressing shRNA specific for the p16 isoform–encoding sequence of *CDKN2A* (as meant by 'p16 shRNA') and were then infected with the pBabe-MycER virus and named B1389-shp16-MycER ($HMEC^{MYC\text{-}ER}$) cells, as previously described[27,28]. Although expression of p16 shRNA delays senescence, the cells are not immortalized and undergo spontaneous senescence when continuously cultured. Therefore, these cells were not used beyond 12 passages after their derivation. $HMEC^{MYC\text{-}ER}$ cells were treated with 4-hydroxytamoxifen (TAM) at 500 nM to induce MYC activation. RP (HCC1428 and T47D) cells stably overexpressing MYC have been previously described[1]. No cell line used in this paper is listed in the database of commonly misidentified cell lines that is maintained by the International Cell Line Authentication Committee (ICLAC) (http://iclac.org/databases/cross-contaminations/). All lines were found to be negative for mycoplasma contamination.

Immunoblot analysis. Proteins were extracted using RIPA buffer (50 mM Tris-HCl pH 7.6, 150 mM NaCl, 0.5% sodium deoxycholate, 1% Triton X-100, 0.1% SDS, 2 mM EDTA) and proteinase (Roche) plus phosphatase (Roche) inhibitor cocktails. Protein extracts were resolved using 4–12% SDS-PAGE gels (Life Technologies) and transferred to nitrocellulose membranes (Life Technologies). Membranes were probed with primary antibodies overnight on a 4 °C shaker, then incubated with horseradish peroxidase (HRP)-conjugated secondary antibodies, and signals were visualized with ECL (Bio-Rad). The primary antibodies targeting the following proteins were used: β-actin (actin) (sc-47778 HRP, Santa Cruz, 1:10,000), PGC-1α (ab54481, Abcam, 1:500), BBOX1 (WH0008424M1, Sigma-Aldrich, 1:500), CPT2 (ab71435, Abcam, 1:500), FASN (SAB1403807, Sigma-Aldrich, 1:1,000), pACC1/2 (11818, Cell Signaling, 1:1,000), ACC1 (4190, Cell Signaling, 1:1,000), ACC2 (8578, Cell Signaling, 1:1,000), AMPK (2532, Cell Signaling, 1:1,000), pAMPK (2535, Cell Signaling, 1:1,000) and c-MYC (MYC) (ab32072, Abcam, 1:1,000).

ATP and NAD(P)H quantification. To determine the effects of etomoxir treatment on ATP levels, tumor cells were seeded in 96-well plates at 5,000–7,000 cells per well and cultured in the presence of 0 or 200 µM etomoxir (Sigma-Aldrich) for 48 h, with triplicate samples for each condition. Relative ATP concentrations were determined using the CellTiter-Glo Luminescent Cell Viability Assay (Promega). To determine the effects of etomoxir treatment on NAD(P)H levels, $HMEC^{MYC\text{-}ER}$ cells were seeded in 96-well plates at 2,000 cells/well and cultured in the presence of 0 or 500 nM TAM for 48 h, then with 0 or 200 µM etomoxir for 24 h, with six samples for each condition. Relative NAD(P)H concentration was determined using CellTiter-Glo 96 AQueous One Solution Cell Proliferation Assay (Promega).

Fatty acid oxidation assay. To determine relative fatty acid oxidation pathway activity, tumor cells were seeded in 24-well plates at 100,000 cells/well in

© 2016 Nature America, Inc. All rights reserved.

triplicate. Cells were incubated in serum-free medium for 2 h and then incubated in standard medium for 1 h. [^{14}C]oleic acid (Moravek Biochemicals, MC406) at 0.1 μCi/μl was added, 2 × 2 cm squares of Whatman paper were taped over the wells, and the cells were incubated for 3 h at 37 °C. After adding 200 μl 3 M NaOH directly to each square of Whatman paper, 100 μl 70% perchloric acid was added to each well and CO_2 was captured at room temperature for 1 h. The Whatman paper was dried at room temperature and placed in a scintillation vial with 5 ml scintillation fluid. ^{14}C radioactivity was measured using a liquid scintillation counter and normalized to protein concentration.

RNAi knockdown. *MYC*-specific (L-003282-02-0005), *CPT2*-specific (M-008574-01-005) and nontargeting (D-001810-10-20) siRNAs were purchased from GE Dharmacon (SMARTpool, four siRNAs per gene). 30 pmol siRNA was used to transfect cells with the Lipofectamine RNAiMAX Transfection Reagent (Life Technologies), according to the manufacturer's instructions. Cells were incubated with siRNA for 72 h. For siMYC studies, medium was changed at 24 h, and 0 and 200 μM etomoxir was added for 48 h before ATP levels were quantified as described above. For siCPT2 studies, the relative number of cells was determined at 72 h as described below.

The *CPT1*-knockdown data was extracted from the Project Achilles data set[17]. The viability score represents the ATARiS solution, which is the computationally derived score that quantifies the gain or loss of growth specific to knockdown of the gene from pooled shRNA screens.

Proliferation and viability assays. To determine the effects of etomoxir treatment on cell proliferation, cells were seeded in 6-well plates at 100,000–150,000 cells/well and cultured in the presence of 0 or 200 μM etomoxir. Cells were harvested at 24, 48 and 72 h. Cell counts were determined using the Countess Automated Cell Counter (Life Technologies) according to the manufacturer's instructions. Cell viability was assessed by performing the flow cytometry–based Guava ViaCount viability assay (Millipore) according to the manufacturer's instructions. To determine the effects of siCPT2 treatment on cell proliferation, cells were seeded in 6-well plates at 100,000–150,000 cells per well and transfected with siNT or siCPT2 as described above. Cells were harvested at 24, 48 and 72 h, and cell counts were determined using the Countess Automated Cell Counter (Life Technologies) according to the manufacturer's instructions. Three independent biological replicates were performed for each time point and condition.

Matrix detachment assays. To determine the effects of matrix detachment, cells were seeded in ultra-low adhesion round-bottom 96-well plates at 1,000 cells/well. Sphere formation was judged by bright-field imaging 4 d after seeding, and then spheres were subsequently cultured in 0 or 200 μM etomoxir for 48 h, with triplicate samples for each condition. Relative ATP concentrations were determined as described above.

Glucose-starvation assays. To determine the effects of glucose starvation, cells were seeded in 96-well plates at 5,000–7,000 cells/well and cultured in replete medium, glucose-depleted medium, 200 μM etomoxir or glucose-depleted medium with 200 μM etomoxir for 24 h, with triplicate samples for each condition. Relative ATP concentration was determined as described above.

Orthotopic allograft and xenograft studies. 4-week-old WT FVB/N and immunocompromised NOD/SCID female mice were purchased from Taconic Biosciences. The derivation of HCI-002 and HCI-009 TN patient–derived xenograft tumors has been previously described[22]. Viably frozen MTB-TOM, HCI-002 and HCI-009 tumor samples were transplanted into the cleared mammary fat pads of FVB/N and NOD/SCID mice, respectively. Tumor growth was monitored daily by caliper measurement in two dimensions. Researchers were not blinded to the treatment groups.

For the [^{13}C]palmitate experiment (**Fig. 1c**), tumors were allowed to reach ~1.5 cm^3, and then the mice were randomized into experimental groups. Mice received 100 mg/kg [^{12}C]palmitate or [^{13}C]palmitate, delivered by i.p. injection at t = 0 h. The palmitate solution was prepared by sonication into PEG-40 (Spectrum). Mice were euthanized at t = 4 h, following which tumors and contralateral non-tumor mammary glands were flash-frozen in liquid nitrogen.

For the HCI-002 acute etomoxir-treatment experiment (**Fig. 4b**), tumors were allowed to reach ~1.5 cm^3, and mice were then randomized into experimental groups. Mice received vehicle or 60 mg/kg etomoxir, delivered by i.p. injection, at t = 0 and 24 h. Mice were euthanized at t = 26 h, and the tumors were flash-frozen in liquid nitrogen.

For the remaining *in vivo* studies, tumors were allowed to reach ~1 cm^3; mice were then randomized into experimental groups, and drug treatment was initiated. For the MTB-TOM studies (**Fig. 4d**, **Supplementary Fig. 9** and **Supplementary Table 6**), mice received vehicle or 20 or 40 mg/kg etomoxir, delivered by i.p. injection, daily for 14 d. Tumor growth was monitored daily by caliper measurement. Mice were euthanized after 14 d of treatment or after tumors reached 2 cm in any dimension, following which the tumors were flash-frozen in liquid nitrogen. For the HCI-002 and HCI-009 studies (**Fig. 4e**,**f**), mice received vehicle, 40 or 60 mg/kg etomoxir, delivered by i.p. injection, daily for 21 d. Tumor growth was monitored daily by caliper measurement. Mice were euthanized after 21 d of treatment or after tumors reached 2 cm in any dimension; for the HCI-002 study, two pieces of tumor from separate locations were fixed in 4% paraformaldehyde (n = 5 for vehicle; n = 7 for 40 mg/kg; n = 4 for 60 mg/kg). The remaining tumor tissue was flash-frozen in liquid nitrogen.

Immunohistochemical analysis. PFA-fixed tumor samples were paraffin-embedded, and a tissue microarray of HCI-002 tumors was created using two 2-mm punch cores per tumor. Immunohistochemical staining of tissue microarrays for Ki-67 was performed using the MIB-1 antibody clone (1:50 dilution; DAKO, Carpinteria, CA, USA), after 20 min of antigen retrieval with epitope-retrieval solution 2 (Leica Biosystems, Buffalo Grove, IL, USA). Images were scored as the percentage of Ki-67$^+$ tumor cell nuclei per total tumor cell nuclei in each captured field using Immunoratio software (http://jvsmicroscope.uta.fi/immunoratio/). TUNEL staining was performed using the ApopTag Peroxidase *In situ* Apoptosis Detection Kit (Millipore) according to the manufacturer's instructions. Images were scored as the total number of TUNEL$^+$ cells per captured field. All quantification was performed in a fashion that was blinded to treatment group.

Statistical analysis. Prism software was used to generate and analyze Pearson correlations (**Fig. 3f**) and the survival plot (**Fig. 4e**). Correlation P values were generated using a two-sided t-test. Clade-enrichment P value was generated using a Fisher's exact test. Survival plot P value was generated using a log-rank test. All differential metabolite abundance and gene expression analyses were performed using the 'limma' R package.

Differential metabolite abundance between MTB-TOM tumors and non-tumor mammary glands was performed using the limma R package[29]. Metabolites that were significantly different between these groups at a false-discovery rate of 0.05 were extracted for downstream analyses. Pathway enrichment within this set of metabolites was quantified using the 'MaxMean' method within the 'piano' R package[30], based on annotations from the Kyoto Encyclopedia of Genes and Genomes (KEGG; http://www.genome.jp/kegg/). Significantly enriched pathways were identified at a P value cutoff of 0.05.

For all other comparisons, unpaired two-sided t-tests were used (GraphPad). No statistical method was used to predetermine sample size. The investigators were not blinded to allocation for the *in vivo* experiments. The investigators were blinded to allocation for immunohistochemical analyses. For all *in vivo* studies, mice were randomized to treatment groups when tumors reached a predetermined volume on a per experiment basis, as described above. For each data set, the data meet the assumptions of the statistical test used, as determined by distribution and variance.

The sample size for all experiments (*in vitro* and *in vivo*) was not chosen with consideration of adequate power to detect a prespecified effect size. For *in vitro* studies, all completed experiments are reported. For *in vivo* studies, the number of indicated mice represents the total number of mice treated and processed for each experiment. No samples were fully processed for metabolomic, western blot, or immunohistochemical analysis and then excluded. For the etomoxir-treatment studies, mice were euthanized at the ethical endpoint (~2 cm) or at the study endpoint, unless they failed to meet the predetermined UCSF Institutional Animal Care and Use Committee quality-of-life guidelines. No mice that completed the studies were excluded from analyses. In the prolonged

© 2016 Nature America, Inc. All rights reserved.

doi:10.1038/nm.4055

PDX-etomoxir study (**Fig. 4e**), two mice from the vehicle group and one mouse from the 60 mg/kg experimental group were found dead of unknown causes, and these tumors were not included in further analyses.

Code availability. Publicly available data sets were acquired as noted. Our annotations of the data sets are available (https://bitbucket.org/jeevb/brca). All code used for this project has been deposited to Github (https://github.com/snjvb/fam_study).

23. Davis, S. & Meltzer, P.S. GEOquery: a bridge between the Gene Expression Omnibus (GEO) and BioConductor. *Bioinformatics* **23**, 1846–1847 (2007).
24. Langfelder, P. & Horvath, S. WGCNA: an R package for weighted correlation network analysis. *BMC Bioinformatics* **9**, 559 (2008).
25. Langfelder, P. & Horvath, S. Fast R functions for robust correlations and hierarchical clustering. *J. Stat. Softw.* **46**, i11 (2012).
26. Mukhopadhyay, R. *et al.* Promotion of variant human mammary epithelial cell outgrowth by ionizing radiation: an agent-based model supported by *in vitro* studies. *Breast Cancer Res.* **12**, R11 (2010).
27. Narita, M. *et al.* Rb-mediated heterochromatin formation and silencing of E2F target genes during cellular senescence. *Cell* **113**, 703–716 (2003).
28. Littlewood, T.D., Hancock, D.C., Danielian, P.S., Parker, M.G. & Evan, G.I. A modified estrogen receptor ligand-binding domain as an improved switch for the regulation of heterologous proteins. *Nucleic Acids Res.* **23**, 1686–1690 (1995).
29. Smyth, G.K. in *Bioinformatics and Computational Biology Solutions Using R Bioconductor* (eds. Gentleman, R., Carey, V.J., Huber, W., Irizarry, R.A. & Dudoit, S.) 397–420 (Springer, 2005).
30. Väremo, L., Nielsen, J. & Nookaew, I. Enriching the gene set analysis of genome-wide data by incorporating directionality of gene expression and combining statistical hypotheses and methods. *Nucleic Acids Res.* **41**, 4378–4391 (2013).

© 2016 Nature America, Inc. All rights reserved.